DOI: 10.13009/EUCASS2019-349

Health Monitoring for Cryogenic Tank Foam Insulations on Reusable Rocket Launch Vehicles

Thomas Thiele, Ansgar Marwege and Ali Gülhan
Supersonic and Hypersonic Technology Department of the Institute of Aerodynamics and Flow Technology
German Aerospace Center
Linder Hoehe, 51147 Cologne, Germany
Thomas.Thiele@dlr.de, Ansgar.Marwege@dlr.de, Ali.Guelhan@dlr.de

Abstract

In the frame of the AKIRA-project a reusable booster stage is investigated concerning different technologies for reusable launch systems. One of these technologies is the insulation of the cryogenic fuel tanks for which a health monitoring system is developed at the German Aerospace Centre in Cologne. Damage detection, localization and classification were performed with an artificial neural network trained with a numerical database of thermal simulations which were validated by experiments on insulation samples in a vacuum test facility. Furthermore, a wind tunnel model is build which will be used for a more realistic reproduction of the heat loads.

1. Introduction

Reusable launch vehicles promise to reduce the costs for space transportation systems. In the frame of the AKIRA-project a reusable booster stage, driven by cryogenic hydrogen and oxygen, is investigated concerning different technologies for reusable launch systems [1]. One of these technologies is the insulation of the cryogenic propellant tanks. The insulation significantly reduces the boil-off rates during fueling and up to launch and prevents icing on the outer tank wall. Different insulation concepts exist for cryogenic tanks like vacuum, foam or aerogel insulations, at which foam insulations are most commonly used for expendable launch vehicles like Ariane 5.

The tank and insulation of reusable launch systems are exposed to recurring strong temperature cycles due to heating and cooling of the structures during fueling, flight and re-entry. This can cause different kinds of damages in the insulation material. For foam insulations these damages include delaminations of the insulation from the tank structure or, as a worst case, spalling of insulation parts due to effects like cryopumping. Detection and repair of such damages are important to ensure the insulation reliability for a reusable system. As maintenance work is a driving cost factor for reusable systems, it is beneficial to install a health monitoring system into the insulation that can directly indicate possible damages without the need of intensive investigations during maintenance. Furthermore, the maintenance strategy can be transformed from a time-dependent approach, in which maintenance is carried out at defined time intervals or load cycles, to a condition-dependent procedure, whereby not predefined cycles are decisive for maintenance and repair, but the actual condition of the structure which leads to a reduction in maintenance and repair costs [2].

Although several insulation concepts are investigated in the AKIRA-project, the health monitoring is focused on foam insulation which is the most promising concept. Different kinds of sensors were investigated for the application as health monitoring sensors in the foam insulation at cryogenic temperatures. Finally, temperature sensors were chosen to detect possible damages in the insulation via changes in the temperature distribution caused e.g. by delamination of the insulation from the tank structure.

A test facility consisting of a small vacuum chamber with integrated sample holder was built to perform tests on rigid foam insulation samples. The holder is cooled using liquid nitrogen to create the necessary cryogenic temperatures. The upper side of the sample can be heated with a silicone heating foil to simulate the outer surface temperature during flight. The samples were instrumented with several thermocouples to monitor the temperature distribution inside the insulation.

To simulate a delamination from the tank structure, a gap between insulation and liquid nitrogen tank was created manually during sample manufacturing. Comparing measurements with and without damage then indicates the temperature change due to a delamination. The measurements were also used to validate corresponding numerical models. Using thermal simulations, further test cases were computed varying parameters like delamination area to create a numerical database for various damage cases. Final damage detection, localisation and classification were then done by an artificial neural network which was trained using the numerical database.

DOI: 10.13009/EUCASS2019-349

In addition to the tests with small rigid foam samples, a wind tunnel model is constructed incorporating a small liquid nitrogen tank, the foam insulation and an additional thermal protection (alumina fibre mat and Inconel steel sheet) on top of the insulation. The model will be tested in an arc-heated wind tunnel at DLR Cologne simulating the convective heating of the outer surface during flight.

2. Defects in Foam Insulations and Possible Health Monitoring Systems

Foam insulations are common for launch vehicles with cryogenic propellants (e.g. Ariane 5 or the Space Shuttle external tank). The materials used for the hydrogen tank of the space shuttle were Polyisocyanurate and Polyurethan. The foam was sprayed on the tank with a thickness of approximately 25 mm.
Especially when the foam application is performed manually, defects can already occur during the spraying process. Typical defects are entrapped air, so-called “rollover voids” (see Figure 1a) or voids (see Figure 1b), cracks caused by stresses in the foam material (see Figure 1c) and delamination of inhomogeneous layers inside the foam insulation (see Figure 1d). However, defects occurring during the manufacturing process can be minimized by machine application of the foam material.
In addition to the defects already occurring during production, damages can also occur during tank operation, e.g. detachment of the foam material from the tank wall and cracks in the foam insulation itself. These damages can, for example, be caused by aerodynamic and thermal loads during flight, vacuum effects, vibrations and mechanical stresses. Other well-known damage mechanisms are so-called "cryopumping" and "cryoingestion".
Cryopumping occurs when a crack in the foam material leads to a void directly at or near the tank wall of the cryogenic tank. Due to the extremely low temperatures of the tank, the air in the void can liquefy and the resulting vacuum can draw in even more air. During take-off and flight the temperatures in the insulation rise due to aerodynamic heating and falling cryogenic fuel levels. This causes the air to evaporate again and pressure forms inside the void which can lead to spalling of foam insulation parts [4].
Cryoingestion follows the same principle as cryopumping. However, instead of air, nitrogen leaks from the inert gas tank into a void near the hydrogen tank and liquefies or freezes.

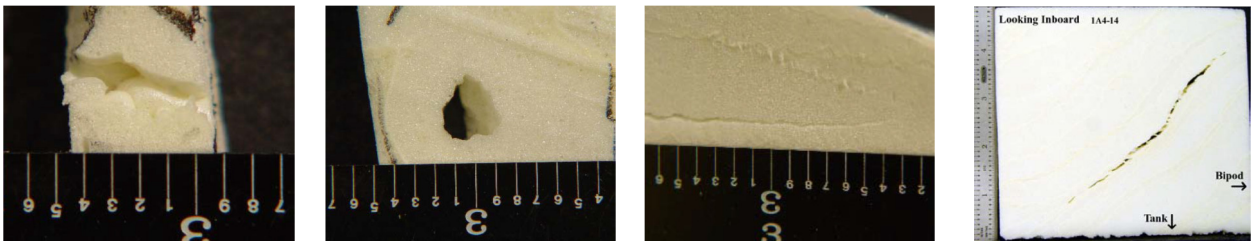

a) Rollover void b) Void c) Crack d) Delamination

Figure 1: Different defects in foam insulation materials [3]

There are several potential approaches for health monitoring of foam insulations:

1) Damages can be visualized using imaging techniques (cameras).
2) With acoustic methods (ultrasound) damages can be detected and localized.
3) Analogous to the acoustic method, X-ray backscatter and electromagnetic waves in the terahertz range can be used for damage localization.
4) Defects in the insulation lead to temperature changes. Therefore, damages can also be inferred from temperature measurements.

With video cameras it is possible to monitor the outer surface of an insulation and to detect large defects such as spalling of insulation parts or large cracks. However, the detection is limited to larger defects that are visible from the outside. A delamination of the insulation from the tank structure, which in itself is not necessarily a critical damage but could later lead to larger defects like spalling of insulation parts, cannot be detected.
Ultrasonic measurements are frequently used in structural health monitoring systems. But in materials with high porosity like foam insulations large acoustic attenuation and scattering occurs [5]. Alternatively a holographic radar using microwaves is proposed in [5] for the inspection of foam insulations. However, this system is not applicable for in-situ measurements during flight.
In the same manner imaging techniques like backscatter X-ray, terahertz and shearography systems, used for the inspection of the space shuttle tank insulation [3], are not suitable for in-situ measurements. But these techniques

DOI: 10.13009/EUCASS2019-349

could be used during maintenance for a more detailed inspection of areas where an integrated health monitoring system detected an anomaly.
Delaminations or cracks can also be detected via changes in the local temperature distribution. In contrast to the above-mentioned systems, temperature sensors can easily be integrated into the insulation to perform in-situ measurements. They are also lightweight, robust and inexpensive. Therefore, temperature sensors were chosen to be used for the health monitoring of the insulation.
The number of necessary sensors per area depends on the required minimum detectable size of a defect. Minor delaminations only influence the temperature distribution in a small area and therefore a large number of sensors would be necessary to detect them. However, in general small delaminations are acceptable and do not influence the insulation performance or lead to spalling of insulation parts, so that a detection of minor defects is not necessary.
There are several types of available temperature sensors like thermocouples or fibre optical sensors. The latter are considered to be embedded in CFRP composites for structural health monitoring (temperature and strain) of aerospace structures and for hydrogen leakage detection at cryogenic tanks [6], [7], [8]. Fibre optical sensors have several advantages: They are lightweight, immune to electromagnetic interference, chemically inert and intrinsically safe since they cannot produce arcs or sparks which is especially advantageous for hydrogen applications. In addition several temperature measurement locations can be combined in one optic fibre. On the other hand optical fibres are fragile which makes them susceptible for damages during integration. Furthermore, the necessary electronics for processing the optical signals to temperature values is much more complex than for other temperature sensors.
Because the mentioned advantages are not important for tests with foam insulation samples using liquid nitrogen, standard thermocouples were used for sample instrumentation because of easier integration and signal processing.
However, as the temperature measurement method is not crucial for the actual health monitoring, also fibre optic sensors could be used for later tests, larger demonstrators or final application.

3. Test Facility for Foam Insulation Sample Tests

Figure 2 shows the thermal vacuum test facility used for foam insulation sample tests. The insulation sample with dimensions of approx. 100 x 100 mm is bonded to an aluminium plate with STYCAST 2850FT epoxy resin which has good adhesive properties and a comparatively high thermal conductivity at low temperatures (≈ 0.9 W/(mK) at 80 K).

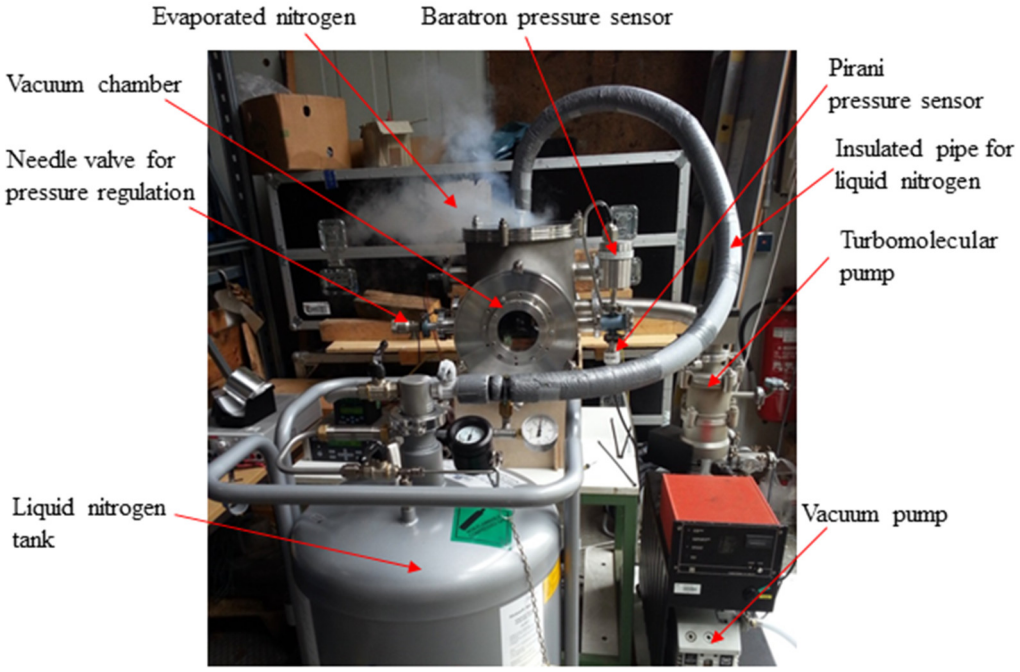

Figure 2: Test facility for foam insulation sample testing

The aluminium plate with the instrumented sample is mounted to the sample holder shown on the left side of Figure 3 with several M5 screws. The sample holder is a stainless steel container which can be filled with liquid nitrogen. The lower side of the container is equipped with a borehole pattern for aluminum plate fixation. The container is connected to the vacuum chamber top cover with four spacers and a stainless steel tube to fill in the liquid nitrogen.

DOI: 10.13009/EUCASS2019-349

The spacers are made of glass-reinforced epoxy laminate material with low thermal conductivity and act as a thermal insulation between container and vacuum chamber.
After fixing the aluminium plate with the foam insulation sample to the holder, the container is inserted into the vacuum chamber as seen on the right side of Figure 3. This figure also shows a copper plate inside the vacuum chamber to which insulation samples can be mounted. The copper plate is connected to a thermostat outside the vacuum chamber with which the plate temperature can be adjusted between -80°C and 200°C. During the tests with liquid nitrogen the copper plate was not used. The liquid nitrogen supply is provided by a tank with a capacity of 100 litres. It is connected to the container inside the vacuum chamber by an insulated pipe. The supply line is not pressure-tight on the vacuum chamber side, so that the nitrogen evaporating during filling procedure and test can escape, see Figure 2.

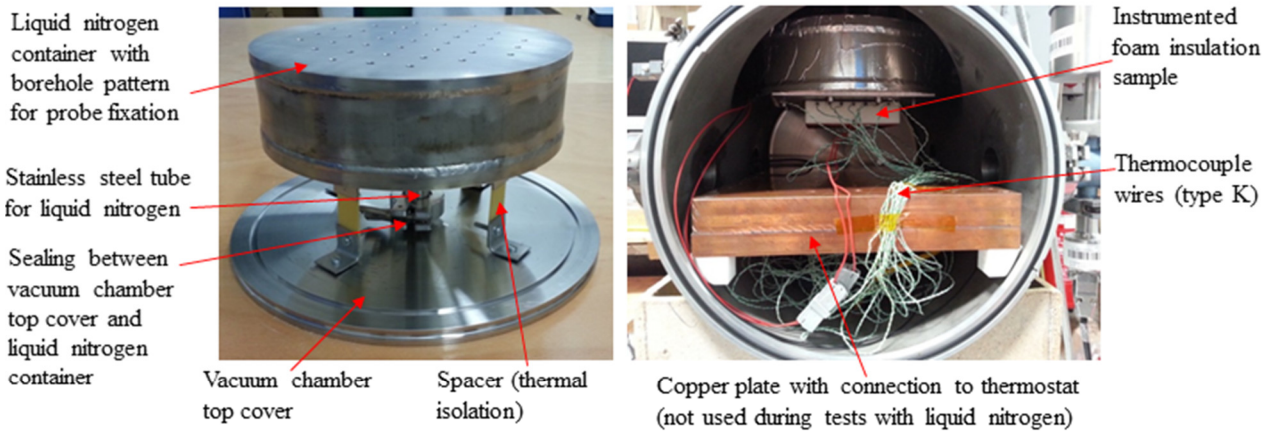

Figure 3: Liquid nitrogen cooled sample holder (left) and sample holder integrated into vacuum chamber (right)

In order to generate the necessary vacuum, a vacuum pump and a turbomolecular pump are connected to the vacuum chamber achieving pressure levels below 10^{-1} Pa. However, a needle valve can also be used to adjust various other pressure levels. The pressure is measured by two sensors. The first sensor is a Pirani sensor with a measurement range down to 10^{-2} Pa. The second sensor is a Baratron absolute pressure sensor of the type 627D with a measurement range of 1300 Pa.
A temperature measurement module from National Instruments (NI-9214) is used to measure the temperatures of the thermocouples inside the foam insulation. This module has 16 analog inputs for thermocouples including cold junction compensation. The module is placed inside the vacuum chamber below the copper plate, so that the thermocouple wires do not have to be led out of the vacuum chamber. The necessary power supply line and the Ethernet communication cable are fed through two vacuum chamber flanges with D-Sub connectors. To supply a heating foil on top of the sample, a 24 V power line is led into the vacuum chamber via a third vacuum chamber flange with D-Sub plugs.

4. Foam Insulation Sample Tests

For the tests in the thermal vacuum facility several different samples were manufactured. One objective of the tests was the verification of the general applicability of temperature measurements inside the foam insulation for health monitoring purposes. In addition the measurements were used to validate a numerical model, especially the used material parameters, see section 5. Because sample manufacturing and tests are very labour-intensive, further test cases were computed using thermal simulations varying parameters like delamination area to create a numerical database for various damage cases. The final health monitoring including damage detection, localisation and classification was then done by an artificial neural network which was trained using the numerical database, see section 6. In order to compare measured temperatures with numerical calculations for model validation, the foam insulation sample manufacturing is essential to be able to accurately reproduce the setup in the numerical model. Inaccuracies in sample production, e.g. in the adhesive joints between thermocouples and insulation, cannot be quantified and are therefore difficult to simulate numerically.
All foam insulation samples were instrumented with eight thermocouples of which seven were distributed equally along the sample width at the same distance to the aluminum plate. The eighth thermocouple was located below the top side of the insulation sample. ROHACELL (110 IG-F) rigid foam insulation with a thickness of 25 mm was used for all samples. This insulation is a candidate material for the propellant tank thermal insulation in the frame of the

DOI: 10.13009/EUCASS2019-349

AKIRA project and was also used in other work packages of this project. All samples were glued onto 3 mm thick aluminium plates, which in turn were screwed onto the liquid nitrogen container (sample holder) as shown Figure 4. Bonding was done with epoxy resin STYCAST 2850FT using catalyst 23 LV.
Type K thermocouples, consisting of twisted thermocouple wires with Polytetrafluoroethylene (PTFE) insulation, were used for temperature measurements. To perform measurements inside the insulation, the thermocouples were inserted into corresponding boreholes to measure the temperatures in the middle of the sample. To ensure good thermal contact between thermocouples and insulation, the thermocouples were bonded to the insulation at the tip.
In order to simulate the heating of the insulation upper surface by heat conduction through the thermal protection system (which is located above the insulation) during flight, a self-adhesive silicone heating foil with a maximum temperature of 150°C was attached to the insulation sample top side. Four thermocouples on the foil were used to monitor its temperature (see Figure 4).
The first tests with the foam insulation samples showed asymmetrical temperature distributions inside the insulation which are not physically reasonable. After varying several parameters like probe size or probe fixation it turned out that inaccurate thermocouple bonding was the reason for the measured asymmetrical distribution. With foam insulation sample RC09 a symmetrical temperature distribution was achieved. A picture of this sample mounted to the sample holder and a corresponding drawing indicating the thermocouple positions are shown in Figure 4.

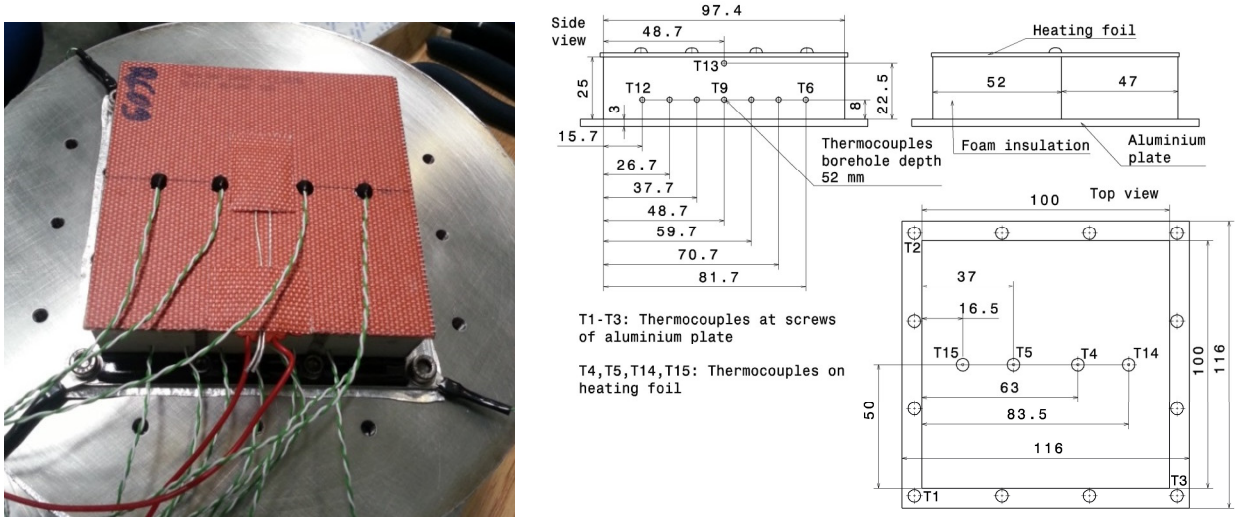

Figure 4: Instrumented foam sample RC09 on sample holder (left) and foam sample instrumentation (right)

The temperature curves measured during the test with sample RC09 are shown on the left side of Figure 5. The temperatures in the insulation reached constant values after approximately 60 minutes of test time. The temperatures of the thermocouples T6 - T12 at t=76 min. are also indicated in Table 1. They show the expected symmetrical distribution with a constant temperature in the middle of the insulation (T8 - T10) and a temperature rise towards the sample edge due to radiation from the environment to the insulation sample.
After 77 minutes of test time the heating foil was switched on and set to a power of 9 Watt. After some time the foil temperature reached a nearly constant value between 102°C and 106°C indicated by the thermocouples attached to the heating foil. This temperature represents the limit temperature of approximately 100°C for the insulation material which was specified within the project. At the same time all thermocouples inside the insulation showed an almost identical value of -79°C ± 1°C, see left diagram of Figure 5 (at t=150 min.).
The diagram also shows the temperatures measured on the aluminium plate (T1-T3). After the cool-down process at the beginning of the test, the temperatures were at a constant value of -193°C. The curves also show some small temperature spikes (e.g. at t=40 min.) which indicate the refilling of liquid nitrogen. During the filling process the O-ring seal between liquid nitrogen container and vacuum chamber shown in Figure 3 cools down and gets slightly untight. This leads to a minor increase in chamber pressure which influences the temperature measurements due to the comparably warm entering air. Because the vacuum pumps are switched on during the whole test time, the pressure drops again rapidly when the refilling is finished.
In order to simulate the effect of an insulation detachment from the tank structure, a small defect was integrated in sample RC09 after the test. In general, a detachment of the insulation would interrupt the heat conduction between insulation and tank wall. Since the actual bonding between insulation and aluminium plate was no longer accessible, the delamination was simulated by the removal of a circular piece of the aluminium plate with a diameter of 15 mm (in the middle of the plate). This also interrupts the heat conduction similar to an insulation detachment.

DOI: 10.13009/EUCASS2019-349

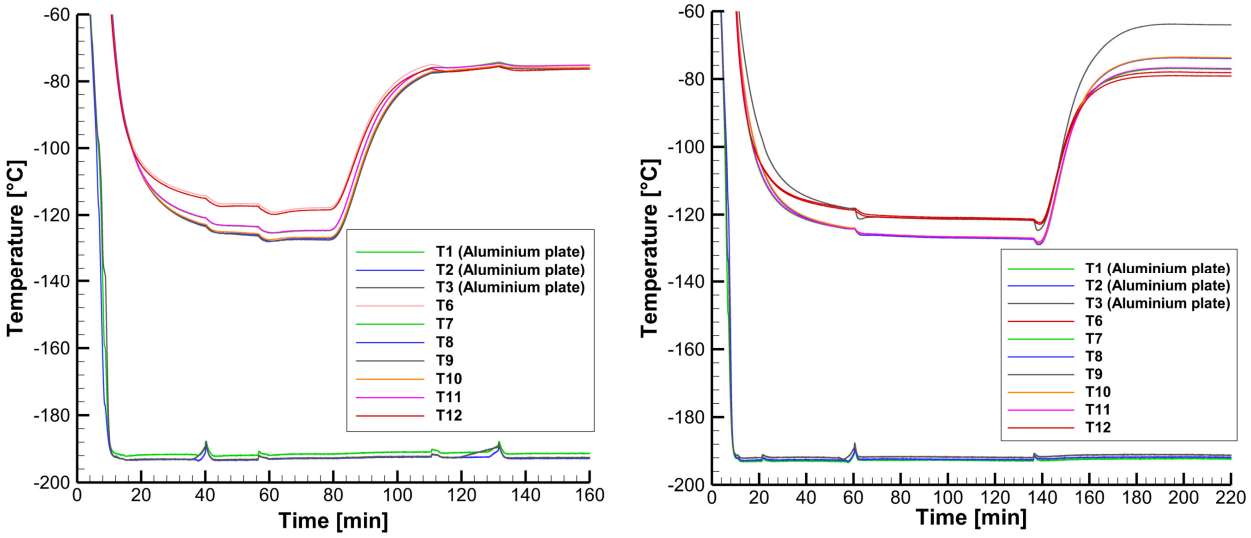

Figure 5: Measured temperature curves during tests with sample RC09 without (left) and with (right) defect

Generally, the interrupted heat conduction causes an increase in temperature in the area above the defect because the heat is less able to flow off to the cold nitrogen container. The temperature change becomes smaller with increasing distance to the defect and is no longer measurable at a certain distance. Whether a defect is detectable via temperature changes depends on the size of the defect and the number and positions of the temperature sensors.
The temperatures curves measured during the test with the defect are shown on the right side of Figure 5. A stationary temperature in the insulation was reached after about 120 min. After approx. 136 minutes of test time the heating foil was switched on with a power of 9 Watt and the foil temperature increased to constant values between 98-102°C. The temperatures inside the insulation (thermocouples T6 - T12) at t=120 min. and t=220 min. are summarized in Table 1.

Table 1: Comparison of temperatures inside the foam insulation sample with and without defect

	T6	**T7**	**T8**	**T9**	**T10**	**T11**	**T12**
Without heating of sample top side (heating foil deactivated)							
Temperature without defect [°C] (t = 76 min.)	-120.7	-127.6	-130	-130.3	-129.6	-127.5	-121.4
Temperature with defect [°C] (t = 120 min.)	-121.3	-127.1	-127.2	-121.7	-126.8	-127	-121.5
Temperature change [°C]	-0.6	0.5	2.8	8.6	2.8	0.5	-0.1
With heating of sample top side (heating foil activated)							
Temperature without defect [°C] (t = 150 min.)	-78.8	-78.5	-79.6	-79.7	-79.3	-78.6	-79.9
Temperature with defect [°C] (t = 220 min.)	-78.1	-77.2	-74	-64.1	-73.7	-76.9	-79.1
Temperature change [°C]	0.7	1.3	5.6	15.6	5.6	1.7	0.8

Based on a measurement accuracy of ± 1.5°C for the thermocouples, the defect could be detected with thermocouples T8 - T10. When the upper side of the insulation is at a higher temperature (heating foil switched on), the temperature change increases due to the larger temperature difference between top and bottom of the insulation.
In this case, a slight influence of the defect can also be seen with thermocouples T7 and T11.
In general, small insulation detachments are only detectable with a high number of temperature sensors because their influence on the temperature distribution is small. Extrapolated to a full-scale propellant tank of a reusable launch vehicle this would result in an unrealistic number of sensors. However, small detachments are not critical and can be tolerated by a real system. Therefore, the damage detection can be limited to larger defects which could eventually lead to critical failures (e.g. spalling of insulation parts). Hence, temperature measurement points can be significantly reduced. In addition, instead of providing health monitoring for the complete tank, it can probably be reduced to highly stressed areas.

DOI: 10.13009/EUCASS2019-349

5. Comparison between Measurements and Numerical Calculations

The presented test with foam insulation sample RC09 was also simulated numerically to check if the results can be reproduced using a simplified numerical model and available material parameters. The following simplifications / boundary conditions were used for the steady-state numerical simulations:

- The heating foil was not simulated as a separate body. It was represented by an adapted emissivity of the upper sample surface. For a powered heating foil a corresponding heat flux was applied to the upper side of the sample.
- The adhesive layer between aluminium plate and insulation was neglected due to the much higher thermal conductivity of the adhesive (λ = 1.02 W/(mK)) compared to the insulation material (λ = 0.032 W/(mK) at 300 K).
- The thermocouples and the liquid nitrogen container were neglected. The temperature of the aluminium plate measured during the tests was used as input for the calculations (T = -193°C).
- A temperature-dependent thermal conductivity was used for the insulation taken from the material datasheet (0.018 - 0.032 W/(mK) between 80 - 300 K).
- All insulation surfaces except the bottom surface radiated to the environment with a constant ambient temperature.

The mesh used for the numerical model can be seen in Figure 6 with 502645 nodes and 292257 elements. A comparison of the measured temperatures with the calculated values for insulation sample RC09 without defect and heating is shown in Table 2. The values show good agreement with deviations in the range of the thermocouple measurement accuracy (± 1.5°C). Only at the edge of the sample (T12) the deviation is higher which is caused by an inaccurately modelled radiation environment at the insulation edges.

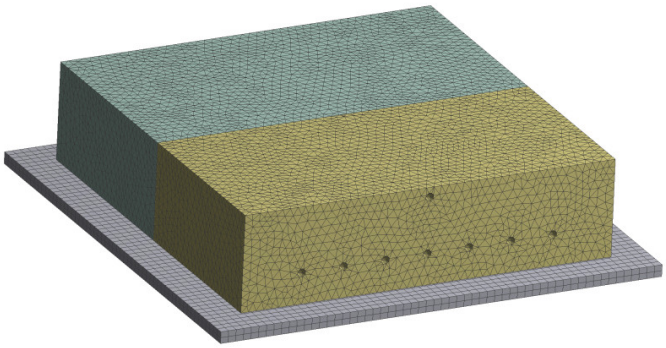

Figure 6: Numerical model including mesh for the foam insulation sample

In the numerical model, only radiation exchange between insulation and environment was assumed with a constant ambient temperature. In the experiment however, a complex radiation exchange takes place between insulation sample, vacuum chamber wall and liquid nitrogen container with non-constant temperatures and temperature-dependent emissivities. Since this is difficult to simulate and the edge influence due to radiation exchange is not present in a real cylindrical propellant tank, a more detailed investigation to minimize the deviation at the sample edges was not conducted.

Table 2: Comparison between measurement and numerical simulation (RC09, without defect, without heating)

Thermocouple	Measurement [°C]	Numeric simulation [°C]	Deviation [°C]
T9	-130.3	-128.6	1.7
T10	-129.6	-128.0	1.6
T11	-127.5	-125.6	1.9
T12	-121.4	-118.0	3.4

Table 3 shows a comparison between calculated and measured values for insulation sample RC09 with defect (see also Table 1). The deviations are slightly higher compared to the test without defect (Table 2) which could be caused by an inaccurate modelling of the defect area. But the deviations are still within the range of the thermocouple measurement accuracy except at the insulation edge due to the radiation exchange.

DOI: 10.13009/EUCASS2019-349

Table 3: Comparison between measurement and numerical simulation (RC09, with defect, without heating)

Thermocouple	Measurement [°C]	Numerical simulation [°C]	Deviation [°C]
T9	-121.7	-119.1	2.6
T10	-126.8	-124.7	2.1
T11	-127.0	-124.8	2.2
T12	-121.5	-117.3	4.2

The comparison of the numerical calculations with the experiments shows an overall good agreement which validates the used material properties for the insulation material. Further test cases were computed using these material properties to create a numerical database for training of the artificial neural network for damage detection.

6. Analysis Tool for Defect Detection and Classification

Detection, localization and size estimation of a possible defect are carried out with a method of machine learning, a so-called Artificial Neural Network (ANN). ANNs are well suited for pattern recognition and evaluation of statistical data. Here, an ANN was chosen because it is easily adaptable to different designs of the SHM system and can be used to simultaneously evaluate and correlate several variables. The inputs for the network are the temperature values of the health monitoring sensors. With this input the ANN shall be able to determine the diameter, height and position of the defect.

6.1 Database of Thermal Computations

For the training of the ANN a large training data set is necessary. It should include all relevant defects and variations of boundary conditions for the temperatures in the foam insulation. Therefore, the training database was created with thermal computations using ANSYS. After training of the analysis tool with numerical data the tool was tested with the experimental data.
For the simulations, a generic configuration of the foam insulation was chosen. A sketch of the configuration is shown in Figure 7a. Similar to the experiments, a 3 mm thick aluminium plate simulates the tank wall with an insulation of 25 mm thickness glued onto it (the adhesive is neglected in the numerical model). The dimensions of the sample are 100 mm x 200 mm. The defect is positioned 50 mm from the left edge of the sample. In this way, the left side with its distance between defect and sample edge corresponds to the experimental setup and is suitable for investigating radiation effects at the sample edge. The right side is further away from the defect and thus simulates an infinite expansion of the insulation.
Theoretically, a defect is defined by three parameters: the diameter of the defect (Diameter Void; DV), the height of the defect itself (Height Void; HV) and the height position of the defect in the insulation (Height Plane; HP). However, since mainly rigid foam insulations in the form of plates are investigated in the AKIRA-project, voids in the insulation plates are unlikely. The more probable case of damage is a delamination of the insulation from the tank wall (HP = 0 mm). Therefore, the parameters to be considered are DV and HV. The different defect cases and boundary conditions for the computation of the database are shown in Table 4.
The defect cases were selected to include the defects investigated in the experiments. The emissivities at the side and the top of the sample were varied, as these material parameters were not exactly known for the used insulation. Additionally, varying the emissivity at the side of the sample down to zero teaches the neural network to neglect radiation effects at the edge which do not appear in an insulation of cylindrical tanks. The theoretical temperature at the bottom of the aluminium plate is -196°C (liquid nitrogen). However, due to effects like a temperature gradient in the liquid nitrogen container or measurement accuracy, approx. -193°C were measured at the aluminum plate during the experiments (see section 4). For robustness of the algorithm against variations in tank temperature it was also varied in the database.
Figure 7b shows the solution of the thermal computation for DV=16 mm and HV=3 mm. In all computations the mesh was refined around the defect to better include its influence on the temperature distribution. Due to symmetry of the configuration a half-model was used to save computational effort. The number of nodes and elements varied for the different defect cases. In the case in Figure 7b the mesh had 37762 nodes and 19981 elements.
A total number of 1332 cases were computed for the database of which 36 cases were reference cases with no defect (DV = 0 mm, HV = 0 mm). For the reference cases the boundary conditions were varied to increase the number of reference cases and enhance the false-alarm-ratio, i.e. the ratio of wrongful detected defects.

DOI: 10.13009/EUCASS2019-349

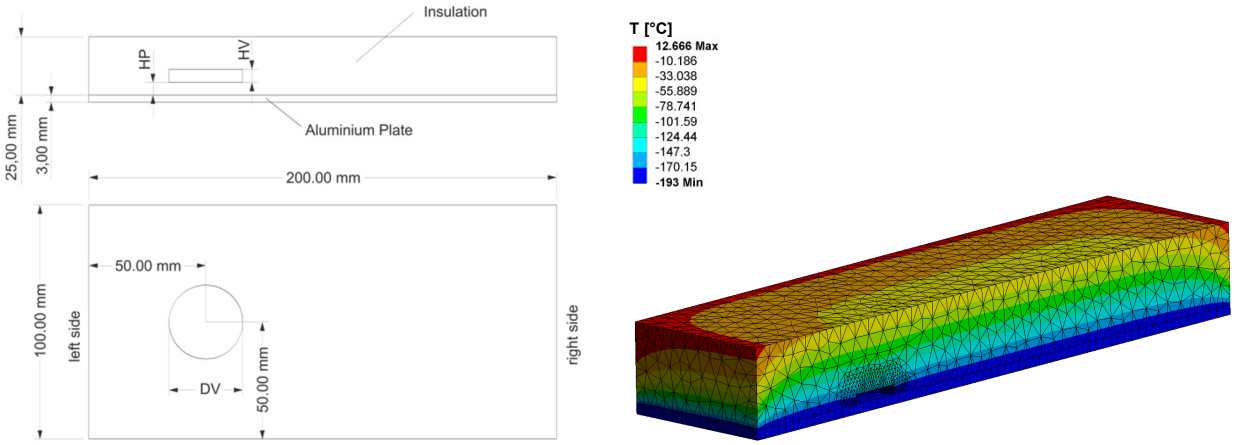

a) Sketch of numerical configuration

b) Result of thermal computation for DV=16 mm, HV=3 mm

Figure 7: Numerical model for the creation of the database

Table 4: Defect cases and boundary conditions for database computations

Defect cases		
Diameter of defect (DV)	[mm]	0, 2, 4, 6, 8, 10, 12, 14, 16, 18, 20, 22, 24
Height of defect (HV)	[mm]	0, 2, 3, 4
Variations of boundary conditions		
Emissivity on sample side	[-]	0, 0.2, 0.3, 0.6
Emissivity on top of sample	[-]	0.4, 0.8, 0.6
Temperature of aluminium plate	[°C]	-180, -193, -196

6.2 Input Data

The input data for the analysis tool are the temperatures at the positions of the health monitoring sensors. To simulate different defect locations, the sensor positions in the numerical model were moved relative to the defect. For the simulation of sensor measurement accuracy a normally distributed temperature error was added to each temperature value. In this way, the data can be easily augmented by defining the number of additional temperature distributions with different measurement errors. The temperature values were then scaled to a range between 0 and 1. For training, testing and validation of the network, the numerical data set was divided into three sub-data sets: training data, test data and validation data.

For the training of the ANN with data similar to the experimental data gained with sample RC09, the input data were extracted at the positions 17, 28, 39, 50, 61, 72 and 83 mm from the left side. As the location of the defect was 48.7 mm in the RC09 sample (middle of sample, see Figure 4) and 50 mm in the database, the positions of the sensors were shifted by 1.3 mm, but had the same relative position regarding the defect. As in sample RC09, temperatures were extracted at a distance of 8 mm from the aluminium plate. The measurement error of the sensors was assumed to be normally distributed with $\mu = 0$ and $\sigma = 0.5$, which corresponds to a measurement accuracy of ± 1.5°C (thermocouples). For each defect case 70 temperature distributions were generated by addition of the normally distributed error. Eighty percent of the data were used for training of the network while 20 percent were used for testing during the training process.

6.3 Output Data

Theoretically, the localization of the defect and the estimation of its extend are regression problems. However, defect locations and defect sizes were discretized. This way the problem was converted to a classification problem. The output data are therefore the labelled and one-hot-encoded defect cases.

DOI: 10.13009/EUCASS2019-349

6.4 Setup

The Keras API [9] was used with the TensorFlow [10] back-end for the construction of the ANN. Its structure for the evaluation of seven temperature sensors and five defect locations is shown in Figure 8. The first layer is an input layer with a dimension according to the number of sensors followed by a fully connected layer (Dense Layer) with the same dimensions. The next layer has a dimension of five times the number of sensors as output. It is followed by another layer which has the same dimensions. The output of this layer is used in sub-networks for the classification of the defect diameter (dense_4 and D_out), the defect height (dense_5 and H_out) and the defect location (dense_6 and Dev_out). The sub-networks each contain a dense layer, which reduces the dimensions from five times the number of sensors to the output dimensions, and an output layer. In total, this network has 2790 trainable parameters. The comparison of several setups showed that hyperbolic tangent activation functions lead to better results than Rectified Linear Unit (ReLu) activation functions. Therefore, the layers dens_1, dens_2 and dens_3 used hyperbolic tangent activation functions. The layers dens_4, dens_5 and dens_6 used ReLu activation functions to avoid the vanishing gradient problem. For the output-layers, “categorical crossentropy” was chosen for the loss function. The softmax-function was selected for the activation function of the output-layers. The Adam optimizer [11] implemented in Keras was used with a learning rate of 0.001.

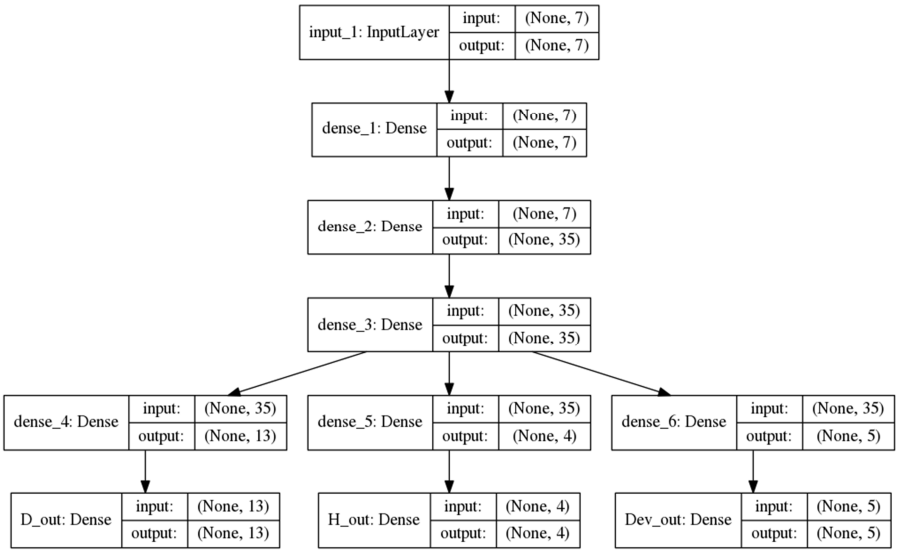

Figure 8: Structure of the neural network for seven temperature sensors

6.5 Test of the Analysis Tool with Experiments

The ANN was trained in three training phases with 200 epochs. The training was performed with the whole training data in each epoch (no batches). The accuracy of the network for the three training phases is shown in Figure 9. It can be observed that after the first 200 training epochs the neural network seems converged. For the second training phase the accuracy only increases slightly and for the third training phase the accuracy keeps nearly constant. The highest accuracy of 83% is reached for the location of the defect (Dev_out). The defect diameter (D_out) is predicted with 70.5% accuracy and the height of the defect (H_out) with an accuracy of 58.7 %. These are the accuracies after testing with the numerical test data set. Table 5 presents the results of the analysis tool applied to the measured temperatures of the tests with insulation sample RC09, see section 4. For all training phases the network correctly identifies in which samples defects are present leading to a false-alarm-ratio of zero. The position of the defect is also correctly detected for all cases. The defect with 15 mm diameter is estimated with 8, 10 and 8 mm for the three training phases. Thus the detection improves after the second training phase but then deteriorates again.
A possible reason could be an over-fitting of the network to the numerical training data. In addition, the probability with which the network indicates the detection decreases during further training phases. Furthermore, the accuracy of the network shown in Figure 9 is not increasing for the third training phase. Therefore, the training should be stopped after the second training phase.
As the defect in insulation sample RC09 was simulated by removing a circular piece of the aluminium plate, the defect did not have a “height” in the insulation. Therefore, the detection of the defect height is not included in Table 5. However, the height is only of secondary interest as for the delamination mainly the defect diameter is important.

DOI: 10.13009/EUCASS2019-349

Table 5 indicates a good agreement between experiment and analysis tool. The defect size is detected correctly concerning the order of magnitude. A changed emissivity on top of the insulation due to the heating foil does not change the response of the ANN, indicating that the emissivity at the top is generalized correctly.
Also the variation of the boundary conditions for the reference case in order to increase the number of cases without defect seems to be a meaningful data augmentation, as the network correctly recognizes samples without defect.
As the analysis tool was only applied on the few available experimental tests, further experiments could be conducted varying defect location and defect size to further validate the analysis tool.
The created numerical database is only valid for the shown insulation layout. For a different insulation setup, like the integrated test object shown in the next section, a new database has to be created for the training of the analysis tool.

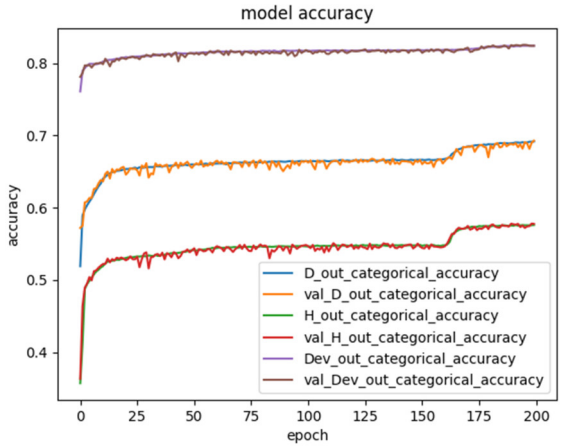

a) First training phase of 200 epochs

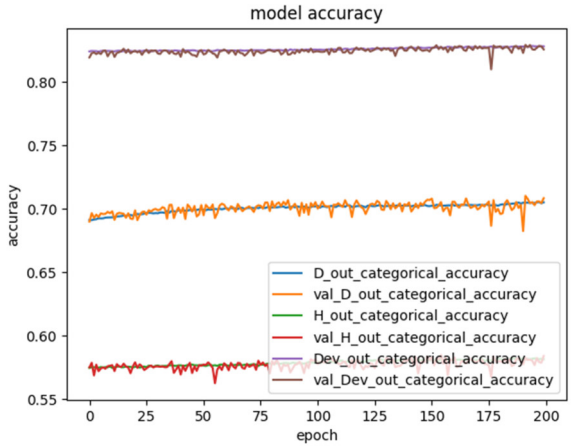

b) Second training phase of 200 epochs

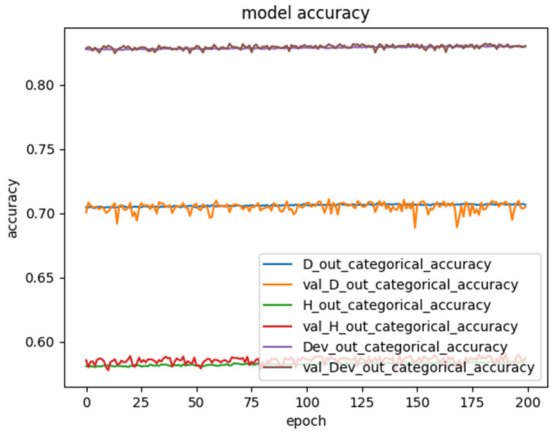

c) Third training phase of 200 epochs

Figure 9: Accuracy of the network after 200, 400 and 600 epochs

DOI: 10.13009/EUCASS2019-349

Table 5: Test of the ANN with experiments

Training phase	Defect	RC09 without heating foil		RC09 with heating foil (switched off)		RC09 with heating foil (switched off) + 15 mm defect	
		Experiment	NN	Experiment	NN	Experiment	NN
1	DV [mm] (probability)	0	0 (98.2 %)	0	0 (95.5 %)	15	8 (96.1 %)
	LD [mm] (probability)	0	0 (93.9 %)	0	0 (94 %)	0	0 (98.4 %)
2	DV [mm] (probability)	0	0 (77.9 %)	0	0 (77 %)	15	10 (77.1 %)
	LD [mm] (probability)	0	0 (99.8 %)	0	0 (99.8 %)	0	0 (99.8 %)
3	DV [mm] (probability)	0	0 (42.3 %)	0	0 (58 %)	15	8 (80 %)
	LD [mm] (probability)	0	0 (93.5 %)	0	0 (96.8 %)	0	0 (99.5 %)

NN: prediction of artificial neural network; DV: diameter of defect; LD: location of defect

7. Integrated Test Object for Arc-Heated Facility

In the frame of the AKIRA-project several integrated test objects are constructed by the project participants (DLR institutes) to test the complete insulation for the cryogenic tank under more realistic conditions. The tank insulation consists of the described foam insulation and an additional thermal protection system on top of the foam insulation as the foam material itself cannot withstand the high wall temperatures occurring during flight and re-entry. A cross-section drawing of the complete tank insulation is given in Figure 10. This layout was developed by collaboration of two project participants [12], [13].

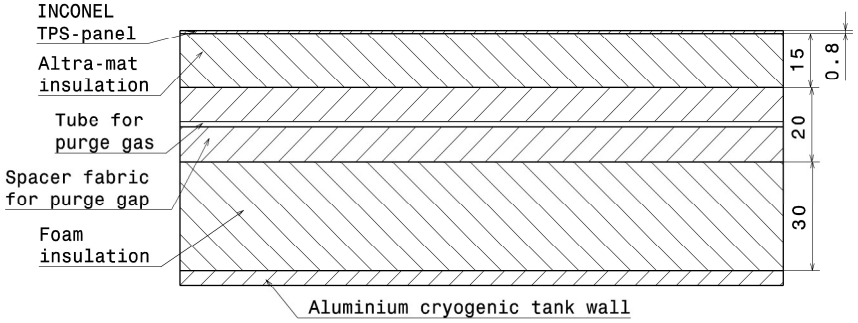

Figure 10: Cross-section of propellant tank insulation including TPS

The foam insulation with a thickness of 30 mm is glued to the aluminium tank structure. Above the insulation a purge gap with a thickness of 20 mm is used which is filled with a spacer fabric made of a fine gas permeable mesh structure. The actual nitrogen purge gas is lead through metallic tubes with several holes, so that the complete gap is filled with the gaseous nitrogen. The purge gap is necessary to prevent icing on the TPS structure during the fuelling process on ground. Without the purge gap the thickness of the foam insulation would have to be increased significantly leading to a too high insulation weight for the reusable launch system. Above the spacer fabric a 15 mm thick alumina fibre mat insulation (Altra) is used with an application temperature up to 1600°C. The mat is covered by a 0.8 mm TPS-panel made of high-temperature INCONEL steel. The whole assembly is fixed to the tank structure with special stand-offs which were designed in the frame of the project [13].
The shown tank insulation structure is able to withstand all occurring temperatures during flight and also prevents icing during fuelling on ground.

DOI: 10.13009/EUCASS2019-349

The test object briefly described in the following is used in an arc-heated wind tunnel at DLR Cologne to simulate the convective heat loads on the TPS during re-entry. All ITOs have the same cross-section layout shown in Figure 10 and use liquid nitrogen to generate the necessary cryogenic temperatures. For the wind tunnel test object no purge gas is used because no purging is performed during flight or re-entry. An overview of the wind tunnel ITO is shown in Figure 11. The model has a length of 327 mm including water-cooled nose and a width of 160 mm. Because of the high gas temperatures in the arc-heated wind tunnel the model support structures including nose, base plate and support arm are water-cooled. The liquid nitrogen container is mounted to the base plate using screws. A lower insulation with a thickness of 21 mm is used between base plate and container to thermally insulate the cryogenic container from the water-cooled structure. The upper insulation layout is identical to the one presented in Figure 10 with one stand-off in the middle of the TPS plate. The TPS panel leading edge is fixed with a small clamping device to ensure a smooth transition between copper nose part and TPS panel and for additional panel fixation. A small tube is used to supply liquid nitrogen to the aluminium container and a second tube is used for the evaporating nitrogen gas. Both tubes are feed through a stainless steel square tube with an internal insulation for protection against the hot gas flow. The tubes are led out of the wind tunnel vacuum chamber to the main liquid nitrogen tank (100 litres capacity, see Figure 2).

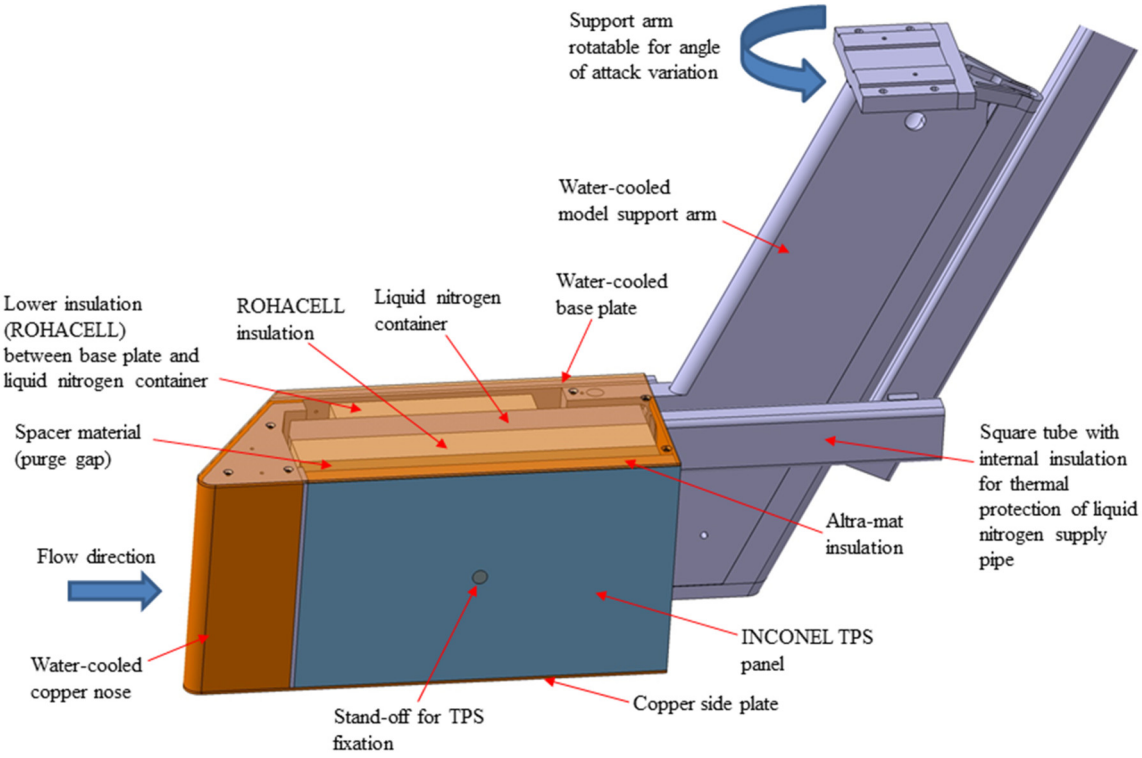

Figure 11: Integrated Test Object (ITO) for tests in arc-heated wind tunnel

The wind tunnel ITO is instrumented with a large number of thermocouples for temperature monitoring of TPS panel, spacer fabric, ROHACELL insulation (including health monitoring sensors), stand-off and liquid nitrogen tank. In addition to the temperature sensors an infrared camera is used to record the surface temperature of the TPS panel.

First tests will be carried out with zero angle of attack to evaluate the temperatures at the TPS. Higher heat fluxes on the TPS panel can be achieved by increasing the angle of attack via the rotatable model support arm. Maximum values above 100 kW/m^2 are possible in the middle of the TPS plate, which is sufficient for the simulation of the heat fluxes occurring at the propellant tanks of the AKIRA reference configuration during flight and re-entry [1].

The manufacturing of the wind tunnel model parts is ongoing at the time of publication and first tests are planned in the second half of 2019.

DOI: 10.13009/EUCASS2019-349

8. Summary

In the frame of the AKIRA-project a reusable booster stage, driven by cryogenic hydrogen and oxygen, is investigated concerning different technologies for reusable launch systems of which one important technology is the thermal insulation for the cryogenic propellant tanks. Due to the vehicle reusability the insulation is exposed to reoccurring thermal cycles and mechanical stresses, which can cause different kinds of damages in the insulation like delaminations of the insulation from the tank structure. Therefore, a health monitoring approach is developed for the tank insulation in the frame of the project which directly indicates possible damages without the need of intensive investigations during maintenance. Although several insulation concepts are investigated in the AKIRA-project, the health monitoring is focused on rigid foam insulation which is the most promising concept. After investigation of possible health monitoring sensors, simple temperature sensors are chosen which detect defects in the insulation via changes in the temperature distribution. As small defects only have minor influence on the temperature distribution and the number of sensors is restricted for a full-scale system, the defect detection is limited to larger defects. However, small defects are not critical and can be tolerated by a real system. In addition, instead of providing health monitoring for the complete propellant tank, it can probably be reduced to highly stressed areas.

To perform tests on foam insulation samples a thermal-vacuum test facility is built which uses liquid nitrogen to provide the necessary cryogenic temperatures. The general applicability of the health monitoring approach is shown using tests performed on foam samples with thermocouple instrumentation. In addition, the measured temperatures are used to validate a numerical model of the insulation setup, especially the foam material parameters. Comparisons between measured temperatures and calculated values show a good agreement. Because sample manufacturing and tests are very labour-intensive, further test cases are computed using thermal simulations varying parameters like delamination area to create a numerical database for various damage cases.

Actual defect detection and classification are done by an analysis tool based on an artificial neural network which is trained to detect defects by changes in the temperature distribution inside the insulation material. The trained analysis tool shows good defect detection accuracy concerning defect location and size when applied to numerical test data. An application of the analysis tool on the experimental data with and without defect shows reasonable agreement. The defect in the foam sample is indicated by the tool and location and size magnitude are detected correctly. But as the analysis tool is only applied on the few available experimental tests, additional experiments varying defect location and defect size would be beneficial to further validate the analysis tool.

The accuracy of the analysis tool strongly depends on the quality of the training data. As a huge amount of experimental tests would be necessary to cover all possible parameter variations, the best way to increase the detection accuracy is a further improvement of the numerical model for database creation.

In addition to tests with small foam samples, a larger integrated test object is constructed incorporating a liquid nitrogen tank, the foam insulation and an additional thermal protection on top of the insulation. It will be tested in an arc-heated wind tunnel at DLR Cologne simulating the convective heating during flight.

In general the numerical database is only valid for the corresponding insulation setup for which it is calculated. Other insulation setups, e.g. the integrated test object, therefore require the creation of a new numerical database for training of the analysis tool.

DOI: 10.13009/EUCASS2019-349

9. References

[1] Sippel, M., S. Stappert, J. Wilken et al. 2019. Focused research on RLV-technologies: the DLR project AKIRA. In: *Proceedings of 8th European Conference for Aeronautics and Space Sciences (EUCASS)*.

[2] Farrar, C., and K. Worden. 2012. Structural Health Monitoring: A Machine Learning Perspective. John Wiley & Sons, LTD. Doi: 10.1002/9781118443118.

[3] Sullivan, R. M., B. A. Lerch, P. R. Rogers, and J. S. Sparks. 2006. An Overview of Spray-On Foam Insulation Applications on the Space Shuttle's External Tank: Foam Applications and Foam Shedding Mechanisms. *Technical report of the 43rd Annual Technical Meeting of the Society of Engineering Science.*

[4] Gehman, H. W., J. L. Barry, D. W. Deal, J. N. Hallock, K. W. Hess, G. S. Hubbard, J. M. Logsdon, D. D. Osheroff, S. K. Ride, R. E. Tetrault, S. A. Turcotte, S. B. Wallace, and S. E. Widnall. 2003. Report of Columbia Accident Investigation Board. Vol. 1.

[5] Ivashov, S.,V. Razevig, I. Vasiliev, T. Bechtel, and L. Capineri. 2015. Holographic subsurface radar for diagnostics of cryogenic fuel tank thermal insulation of space vehicles. In: *NDT&E International.* Vol. 69, pp. 48-54. Doi: 10.1016/j.ndteint.2014.10.002.

[6] Melvin, L., B. Childers, R. Rogowski, and W. Prosser. 1997. Integrated Vehicle Health Monitoring (IVHM) for Aerospace Vehicles. In: *International Workshop, Structural health monitoring*, pp. 705-714.

[7] Graue, R., M. Krisson, M. Erdmann, and A. Reutlinger. 2000. Integrated Health Monitoring Approach for Reusable Cryogenic Tank Structures. In: *Journal of Spacecraft and Rockets.* Vol. 37, pp. 580-585. Doi: 10.2514/2.3630.

[8] Latka, I., W. Ecke, B. Höfer, C. Chojetzki, and A. Reutlinger. 2004. Fiber optic sensors for the monitoring of cryogenic spacecraft tank structures. In: *Proceedings of Photonics North: Photonic Applications in Telecommunications, Sensors, Software, and Lasers.* Vol. 5579. Doi: 10.1117/12.567353.

[9] Cholletand, F. et al. https://keras.io. 2015.

[10] Abadi, M., et al. https://www.tensorflow.org. 2015.

[11] Kingma, D. P., and J. L. Ba. 2015. Adam: A Method for Stochastic Optimization. *3rd International Conference on Learning Representations.*

[12] Darkow, N., A. Fischer, H. Scheufler, H. Hellmann, and J. Gerstmann. 2019. Concept Development of a Cryogenic Tank Insulation for Reusable Launch Vehicle. In: *Proceedings of 8th European Conference for Aeronautics and Space Sciences (EUCASS)*.

[13] Reimer, T., E. Arce, C. Rauh, N. Darkow, and A. Fischer. 2019. Interface Designs between TPS and Cryogenic Propellant Tank of an RLV Booster Stage. In: *Proceedings of 8th European Conference for Aeronautics and Space Sciences (EUCASS)*.